



Effect of Friction Stir Processing on Microstructure and Mechanical Properties of TIG Welded Joint of AA6061 and AA7075

Husain Mehdi¹ · R. S. Mishra¹

Received: 21 November 2019 / Revised: 24 February 2020 / Accepted: 7 April 2020 / Published online: 28 April 2020
© ASM International 2020

Abstract

In tungsten inert gas welding (TIG), micro-cracks, porosity, coarse grain structure and high residual stress distribution were found due to persisting thermal conditions. The TIG welded joint is processed using friction stir processing with input process parameters to avoid these defects. In present work, the experimental investigation was conducted to examine the influence of friction stir processing (FSP) on microstructure and mechanical properties of TIG welded joint of AA6061 and AA7075. Tensile test, Vickers hardness test, x-ray diffraction, microscopy and energy-dispersive x-ray test were performed for concluding the optimum set of parameters. The tensile test results shows that the hybrid TIG + FSP welded joint had higher tensile strength than TIG welded joint with filler ER4043, whereas the increment in the micro-hardness of TIG + FSP welded joint was observed. The grain size also decreases when tool pin rotates on TIG welding with different processing parameters. It was found that the maximum tensile stress, % elongation and micro-hardness at nugget zone for TIG + FSP welded joint are 255 MPa, 29.2, and 105 HV respectively. The present investigation demonstrates that the tool rotational speed and traverse speed are the dominating parameters to improve the mechanical properties of TIG welded joint.

Keywords Tensile strength · Micro-hardness · Residual stress · Microstructure

Introduction

Modern development in the automobile sector and defense sector has been transformed from conventional materials to light material such as aluminum alloy. Due to excellent mechanical and physical properties of aluminum alloy such as high strength, excellent corrosion resistance, low density and high thermal conductivity, it is mostly used for making various components such as military aircraft, rocket, and rocket launcher, axle shafts, rims, bumpers and car bodies [1–2]. The friction stir welding (FSW) is used to fabricate the automotive and shipping components, aircraft structural components and reducing structural weight as shown in Fig. 1. This solid-state welding is used in defense and aerospace [3–5]. Many aluminum alloys like AA2219 and AA7075 have large range of applications in defense; it includes fabrication of fuel tank of cryogenic rocket and ammunition hardware [6–9]. The fusion welding (FW) of

Al-alloy has a prodigious challenges for researcher. The problems associated with aluminum alloys welded joints are aluminum oxide, coarse grain structure, micro-crack, solidification shrinkage and high residual stress [10]. Due to eutectic melting and re-solidification of the fusion zone (FZ), the brittle inter dendritic structure was found, which influence the low tensile strength, ductility and low hardness [11–13]. Therefore, fusion welding has a major defect during welding process. Friction stir welding has many benefits such as low residual stress and distortion, low welding defects and can also weld thick and thin plates. During welding, the thermal stress induced in the material is a big concern, because these stresses affect microstructure, plastic flow and residual stresses. The residual stresses present in weldment have a strong cause on failures and crack on welded joint [5]. The effects of tool feed rate on residual stresses of FSW of Al-alloy joints were studied with synchrotron x-ray measurement and analyze the residual stress in longitudinal and transverse direction [14]. FSW can affect the performance of the residual stresses in the weldment. Due to low heat input, the residual stress in FSW joint is very low. In FSW, the processing parameters may affect the development of residual stresses [15–16].

✉ Husain Mehdi
husainmehdi4u@gmail.com

¹ Department of Mechanical Engineering, Delhi Technological University, New Delhi, India

Many past researchers were studied and investigated about processing parameters of friction stir welding for enhancement of mechanical properties of welded joint [17–23]. Many researchers have been developed the models for predicting the optimized tensile strength FSW welded joint of various aluminum alloy by response surface method [24–26]. Various optimization methods have been used to optimize welding parameters and established empirical relationship between welding parameters and their responses. Most popular methods to solve the optimization problems are RSM using design expert and MINITAB software [27]. The hardness of TIG welded joints was measured to be higher as compared to gas tungsten arc welding (GTAW) due to higher weight percentage of carbon in weld fusion zone [28–29]. Mechanical properties and residual stresses of friction stir welded joint and TIG welded joint of different steel have been studied with various process parameters in different welded zone. The residual stress has been carried out in heat-affected zone and fusion zone by using blind hole drilling method. The residual stress in TIG welded joint was observed higher than friction stir welding. Compressive residual stress was observed in base material, whereas tensile residual stress was observed in heat-affected zone [30].

The effects of rotation speed on microstructure and mechanical properties of welded joints by dual rotation friction stir welding were analyzed and found fine equiaxed recrystallization grains and defect-free joints under various process parameters [31]. A new welding approach of TIG + FSP was successfully applied to the AA2024 to

enhance the mechanical properties of welded joint. They conclude that the defects and porosities in the TIG welded joint are completely reduced by FSP process and modified the microstructure and mechanical properties of TIG + FSP welded joint [32]. The application of FSP on TIG welded joint improved the ductility and tensile strength of welded joint of AA5083-H111, and results revealed best reduced dimple size [33].

This work is focused on to enhance the microstructure and mechanical properties of TIG welded joint of AA6061 and AA7075 by FSP process under various processing parameters. This topic is carefully selected after noticing that there is little literature review available on TIG + FSP welding approach. The outcomes of this paper will give the new approach for enhancing the mechanical properties of TIG welded joint which play a huge role in welded structures.

Material and Experiment Work

The base plates of A6061 and AA7075-T6 of 6.2 mm thickness were used for present experimental work. AA7075 is an Al-Zn-Mg alloy which gains higher strength from the precipitation hardening. The chemical composition of AA6061 and AA7075 obtained by energy-dispersive x-ray spectroscopy (EDX) is presented in Table 1.

The filler wire of ER4043 of diameter 2.4 mm was used to join single V groove plate at voltage 23 V and current 110 amp. Argon (22 lit/min) is used as a shielding gas and travel speed 3.2 mm/sec to fabricate the joint.

After TIG welding, FSP technique was used on TIG weldment to improve the microstructure and mechanical properties of the welded joint. The non-consumable H13 tool steel with pin diameter (octagonal cross section), shoulder diameter and pin length of 7 mm, 19.5 mm and 5.5 mm respectively was used. The input parameters range for TIG + FSP welded joint have been taken as rotational speed (1000 rpm to 1300 rpm), traverse speed (30–60 mm/min) and tilt angles (0° – 2°). Only defect-free TIG + FSP welded joints were further investigated.

Figure 2 demonstrates the dimension of tensile sub test specimen as per ASTM E8. The tensile test specimen was sliced and machined from the welded joint using milling cutter and shaper machine. Single-pass FSP used to fabricate TIG + FSP welded joint is shown in Fig. 3. Three sub tensile specimens were tested on UTM machine at room

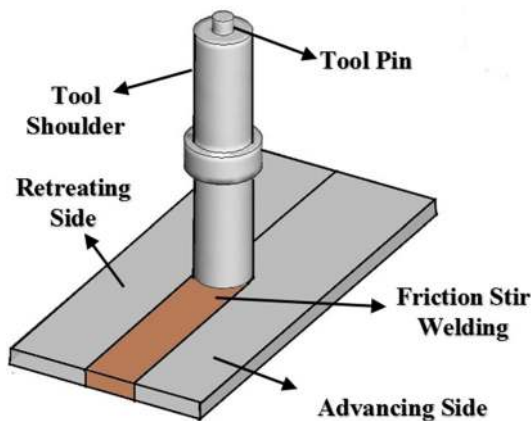


Fig. 1 Friction stir welding

Table 1 Chemical composition of filler wire and parent material

Material	Si	Cu	Fe	Zn	Mg	Mn	Cr	Ti	Al
ER 4043	5.3	0.025	0.8	0.1	0.05	0.02	Bal.
AA7075	0.58	1.2	0.35	5.1	2.1	0.12	0.2	0.05	Bal.
AA6061	0.4–0.8	0.2	0.7	0.25	0.8	0.1	0.2	0.15	Bal.

temperature, and average of these three results is taken. Vickers micro-hardness machine was used for measuring the hardness across the welded joint with a load of 100 g and dwell time 30 s. Microstructure observation was carried

out using scanning electron microscope (SEM) for TIG and TIG + FSP welded joint.

Twenty experiments have been conducted with three independent input variables in which some fabricated joints are shown in Fig. 4. The processing parameters of TIG + FSP and its level are shown in Table 2.

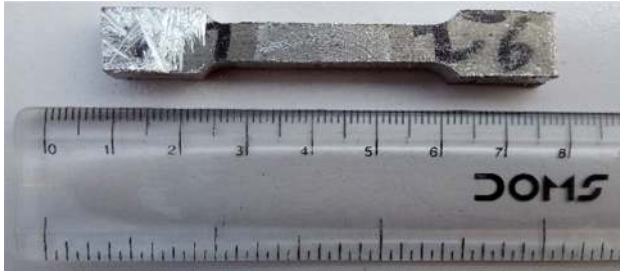


Fig. 2 Dimension of tensile test specimen as per ASTM E8



Fig. 3 FSP process after TIG welding

Results and Discussion

Microstructure Analysis Of TIG And TIG + FSP Welded Joint

The microstructure of TIG welded joint of Al-6061 and 7075 with filler ER4043 was observed at different locations using various magnifications. Figure 5 shows the different zones of TIG welded joint such as welded zone, fusion zone and HAZ. Fusion zone was formed due to re-solidification and melting during the welding. The dispersed precipitates of Mg_2Si intermetallic compound were observed in welded region, and coarse equiaxed grains were also observed in fusion zone. The equiaxed grains absent due to the material close to the fusion line provide plenty of sources for the crystal nucleation of the liquid metal during the TIG welding [34]. Fine grains with small precipitates were reported in heat-affected zone (HAZ) as compared to other zone.



Fig. 4 Various TIG + FSP fabricated joint

Table 2 Processing parameter of friction stir processing and its level

Parameters	Units	Notation	Range	Levels		
				– 1	0	1
TRS	rpm	A	1000–1300	1000	1150	1300
TS	mm/min	B	30–60	30	45	60
TA	degree	C	0–2	0	1	2

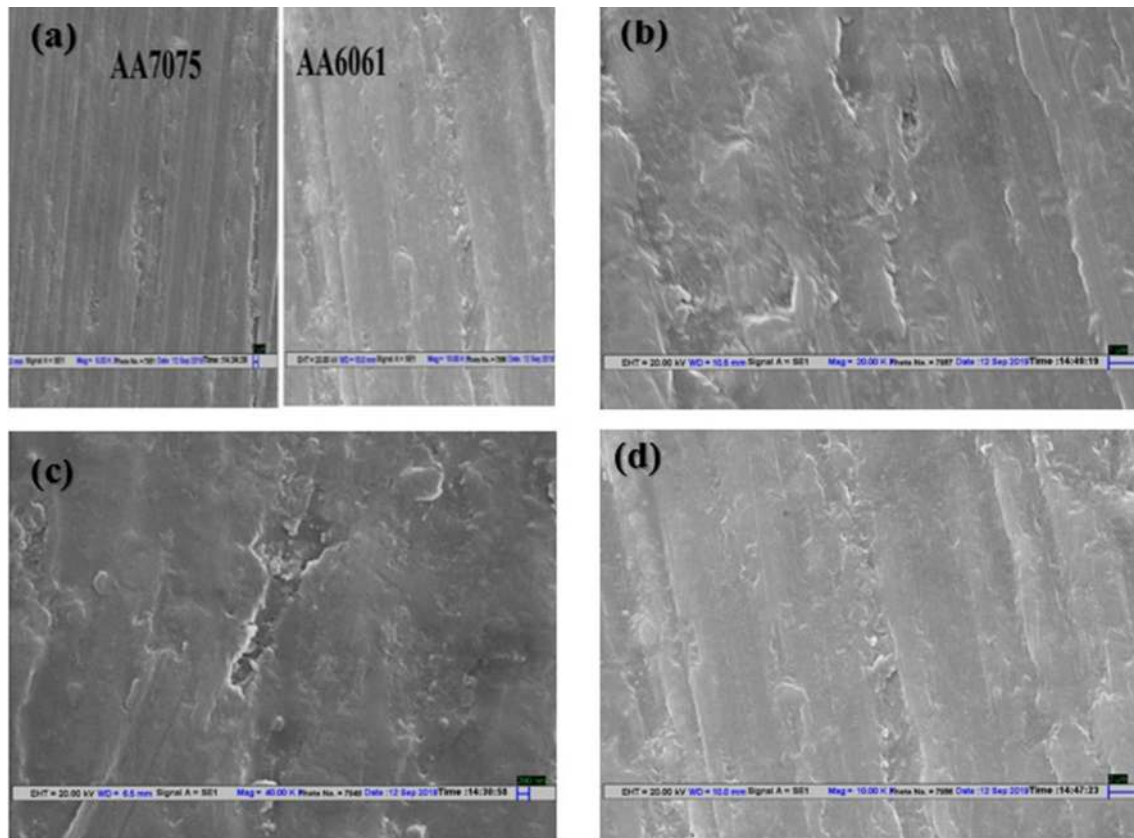


Fig. 5 SEM images of TIG welded joint (a) base material, (b) welded zone, (c) fusion zone, (d) HAZ

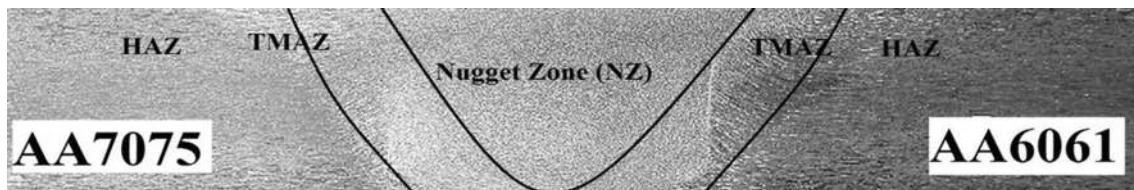


Fig. 6 Optical micrograph of various zone for TIG + FSP welded joint of AA7075 and AA6061

The relationship between heat input and the grain size is measured by electron backscatter diffraction (EBSD) in the stir zone [35]. The mean grain size generally decreased with the heat input under the studies conditions. The revealed relationship was characterized by a significant experimental scattering. This deteriorates their predictive ability and therefore requires a deeper understanding for the heat input and grain growth. The heat input is directly related to the variation of the welding temperature. The final grain size in the stir zone is depended on the peak welding temperature and weakly on the cooling rate [36].

Three different zones have been recognized in TIG + FSP weldment at low magnification due to mechanical and thermal stresses caused by the processing parameters. These zones are nugget zone (NZ), thermo-mechanically affected zone (TMAZ), and heat-affected zone (HAZ) are shown in Fig. 6. The formation of nugget zone shape in TIG + FSP welded joint is recognized to the maximum deformation and plasticization in the material which shows the fine recrystallized equiaxed grains. The formation of nugget shapes depends on thermal gradient, processing parameters and tools geometry in the workpiece [37]. Therefore, coarse grain structure of TIG welded joint is

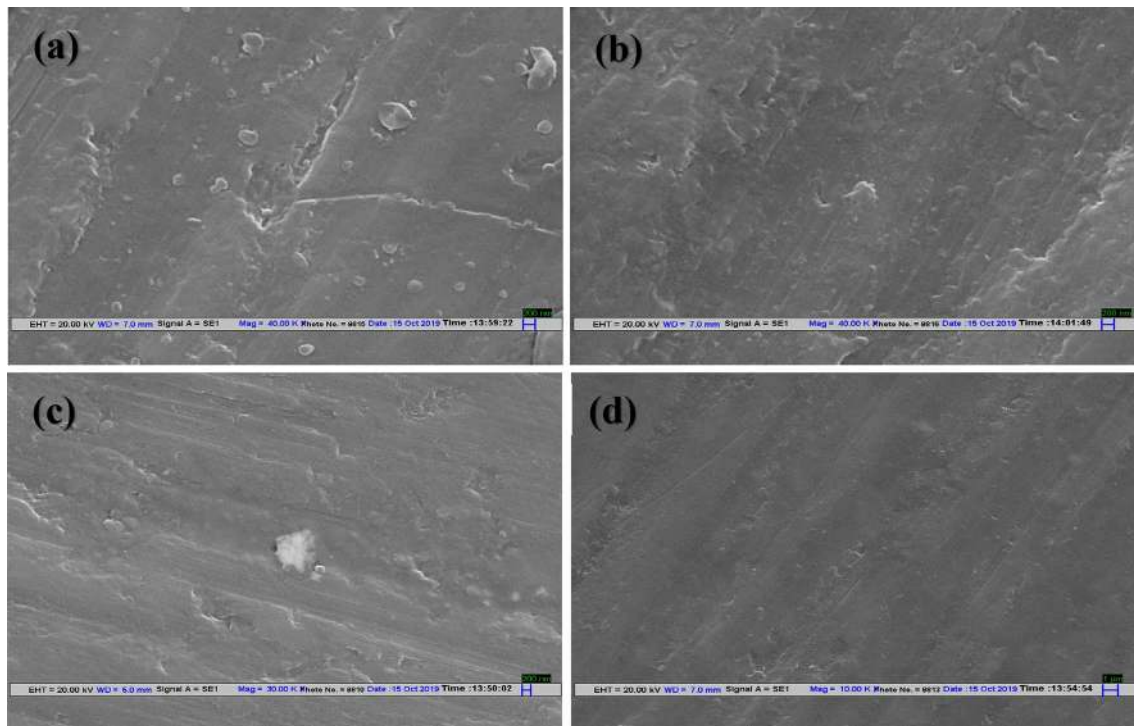


Fig. 7 SEM images of TIG + FSP welded joint (a) sample 1, (b) sample 5, (c) sample 12 and (d) sample 18

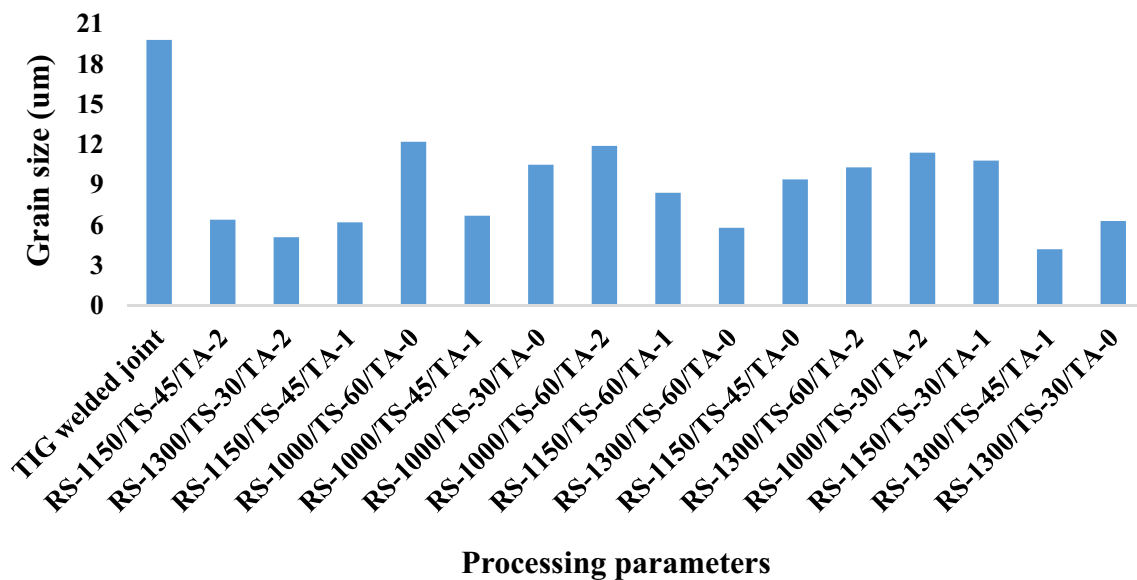


Fig. 8 Variation of grain size at the nugget zone to the processing parameters

transformed into the uniform and fine grains structures in the weld nugget zone due to adequate softening of material revealed the maximum tensile strength and micro-hardness of the TIG + FSP welded joint as shown in Fig. 7. At high welding speed, the weld nugget zone is more homogenous

than those produce low welding speed because high heat input gives the effective recrystallization and more homogenous temperature distribution in weld nugget zone. The grains sizes in stir zone change crucially which is depended on the heat input and processing parameters [38–39]. The grain sizes of TIG weldment were analyzed

by the image J software, and observed grain sizes in fusion zone at three different positions are 19.2 μm , 19.8 μm and 18.5 μm , whereas 5.4 μm , 5.9 μm and 4.2 μm were observed in TIG + FSP welded joint at 1300 rpm, 45 mm/min as shown in Fig. 8.

Fracture Surface Analysis

Fractured surfaces of the fragmented tensile specimens were analyzed by SEM machine to understand the effect of microstructure on the failure pattern of TIG and TIG + FSP welded joints. Some important observation can be made. All TIG welded specimens are failed at the welded joint, whereas most of the TIG + FSP welded joint failed on the advancing side, while some specimens were failed at retreating side because fracture was initiated from the interface of TMAZ and stir zone in retreating side. The reasons for such localized fracture behavior are explained by analyzing the texture, grain size and strain localization characteristics in retreating side [40]. The scanning electron microscope (SEM) fractograph has been taken from the fractured tensile test specimen of TIG and TIG + FSP welded joint of AA6061 and AA7075 at room temperature as shown in Fig. 9. The fracture morphology between

the TIG and TIG + FSP shows the clear difference that TIG welded portion shows the deep dimples, whereas TIG + FSP welded portion shows shallow dimples with fractured lines; this is the evidence of crack nucleation and growth 4 mm away from the weld line. The small grain particles were found in the TIG + FSP welded zone, while big grains were found in TIG welded region. A number of small and big silicon particles are observed in both fractured specimens. Because of formation and consequent growth and coalescence of cavity or voids, the ductile fracture of welded joint occurs; an improvement in ductility may be achieved when the cavity nucleation could be suppressed [41]. The maximum interfacial normal stress depends upon the grain particle size and the volume fraction of the grain particles [42].

Pandey et al. [43–44] have explained that the coalescence of micro-voids results in equiaxed dimples on tensile fracture surface normal to the loading axis. Hence, the equiaxed and spherical dimples on a flat crater bottom loaded in tension and elongated ellipsoidal dimples on the shear lips oriented at 45°.

SEM fractograph of the fractured tensile test specimen shows the size and distribution of large void and cavity of different TIG + FSP welded joint. The fractured surface is

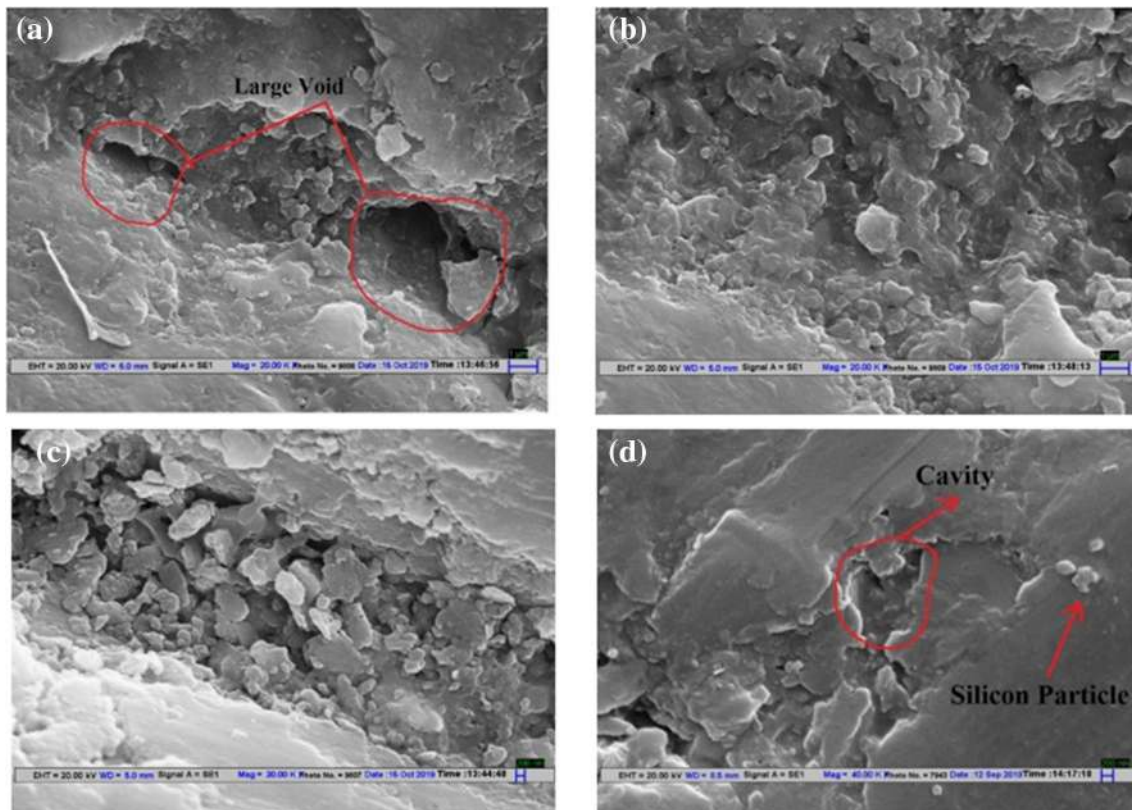


Fig. 9 SEM images of tensile fractured specimen, (a) TIG welded joint, (b) TIG+FSP welded joint (sample 4), (c) TIG+FSP welded joint (sample 9), (d) TIG+FSP welded joint (sample 18),

characterized by ductile dimple and some area of large void as shown in Fig. 9. The fine dimple percentage increases by the variation of process parameters of TIG + FSP welded joint. The cavity formation occurred due to precipitate coarsening that layer coalesce led to the shear rupture.

EDX Analysis

The energy-dispersive x-ray spectroscopy (EDX/EDS) of tungsten inert gas welded joint with filler ER4043, and TIG + FSP welded joint has been analyzed. It was found that atomic percentage of Al and Si in the welded joint is higher than the other elements. Figure 10a illustrates the EDX image, while Table 3 shows the percentage of element concentration at fusion zone (FZ) in TIG welded joint with filler ER4043. The percentage of aluminum being highest (88.3%), Si is 4.58% (2nd highest), and Zn is 2.2% (3rd highest) in TIG welded joint, whereas alloying elements are uniformly distributed in TIG + FSP welded joint as shown in Fig. 10b and Table 4. Zinc (Zn), magnesium (Mg) and silicon (Si) elements were found in the weldment besides the aluminum (Al); it is found that Mg, Zn and Si created

the phase after the precipitation reaction in the weldment. A very high intensity was found from aluminum, because of fragmentation of precipitates the intensity of Mg_2Si and $MgZn_2$ decreases after friction stir processing on tungsten inert gas welded joint.

XRD Analysis of TIG and TIG + FSP Welded Joint

X-ray diffraction is used to examine the phase detection of dissimilar welded joint AA6061 and AA7075 with filler ER4043 and found three major phases Al, Al_2CuMg and Mg_2Si as shown in Fig. 11. Magnesium (Mg) and silicon (Si) elements were found in the weldment besides the aluminum (Al); it is found that Mg and Si created the phase after the precipitation reaction in the weldment. A very high intensity was found from aluminum, because of fragmentation of precipitates the intensity of Mg_2Si increases after friction stir processing on TIG welded joint with filler ER4043 [45–46]. The alloying elements such as Si and Mg existing in weld center make precipitation reaction and form a strong precipitate of Mg_2Si to give a higher strength. Same phase of Al_2CuMg was detected in both the nugget zone.

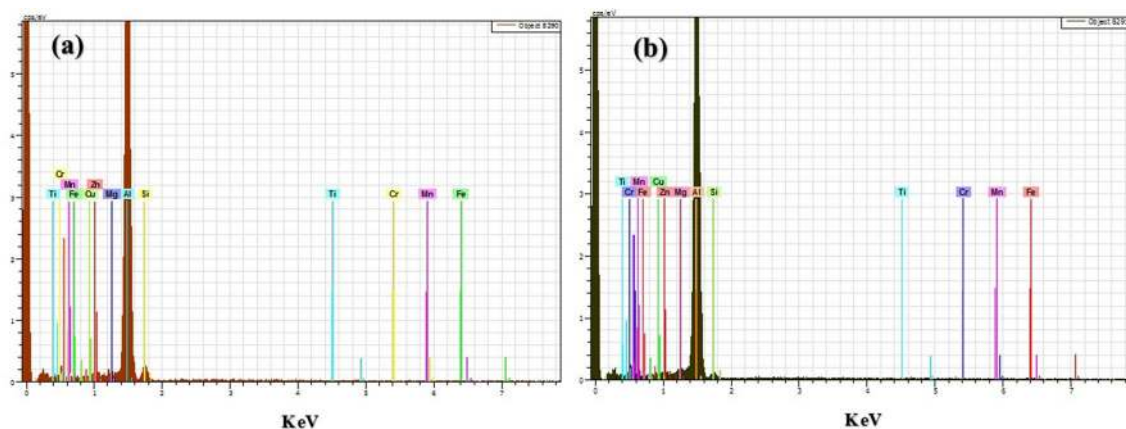


Fig. 10 EDX analysis of (a) TIG welded joint, (b) TIG + FSP welded joint

Table 3 Concentration of elements in TIG welded joint of AA6061 and AA7075 with filler ER4043 at 3 different points

Elements (%)	Al	Si	Zn	Cu	Fe	Mg	Mn	Cr
Point-1	83.1	3.47	2.81	2.62	2.5	1.77	1.25	0.9
Point-2	81.5	5.94	2.61	2.2	2.04	1.88	1.22	0.96
Point-3	88.3	4.58	2.2	1.84	1.72	1.13	0.86	0.47

Table 4 Concentration of elements in TIG + FSP welded joint for sample 18 at 3 different points

Elements (%)	Al	Si	Zn	Cu	Mg	Fe	Mn	Cr
Point-1	85.88	4.94	2.61	1.76	1.64	0.95	0.69	0.49
Point-2	84.63	4.91	2.53	1.58	1.52	1.12	1.08	0.77
Point-3	85.31	4.52	2.23	2.12	1.82	1.03	0.65	0.51

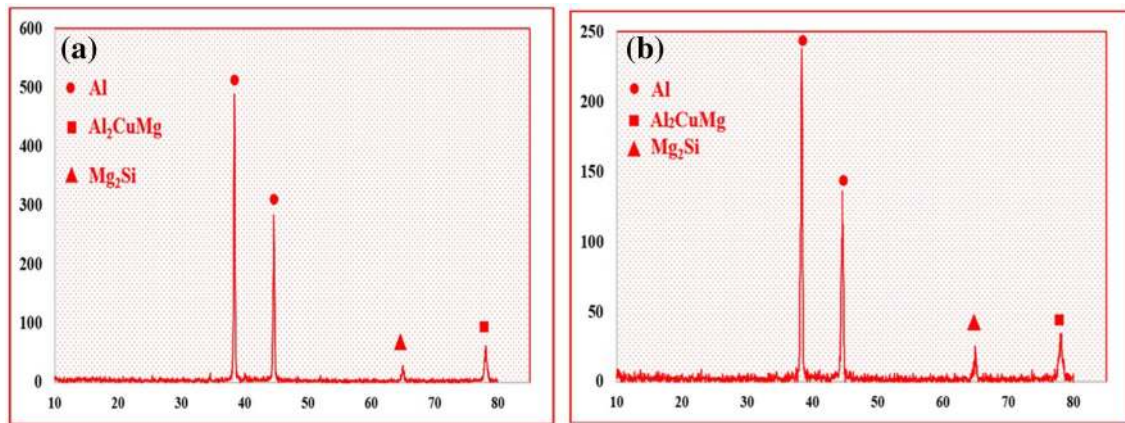


Fig. 11 XRD peaks with filler ER4043, (a) TIG welding, (b) TIG + FSP welding

Micro-hardness of the TIG + FSP joints is based on boundary energy, brittle intermetallic formation, strain hardening and precipitates formation in the joint.

Fine recrystallized grains and increase in grain boundaries in the (SZ) of AA6061 and AA7075 joints predict higher micro-hardness. Because of fine precipitates and fine grains structure, the stir zone is associated with plastic deformation and high temperature, due to precipitates formation at high temperature along the grain boundaries. When the rotational speed of tool is less than the 1000 rpm, the worm hole at R.S was observed due to insufficient of metal transportation and insufficient heat generation in TIG + FSP welded joint, whereas when the TRS is higher than the 1300 rpm, the high heat was observed in the NZ, results widen the HAZ and weaken the microstructure bonds. Pin holes defect was observed at traverse speed less than 30 mm/min due excessive heat input per unit length in the weldment. When feed rate is greater than 60 mm/min, the bottom tunnel in the advancing side was perceived due to inadequate flow of material and insufficient heat input in the weldment.

Tensile Strength

The influences of FSP on TIG weldment were analyzed with the help of computer controlled UTM machine at room temperature using different processing parameters. According to the hall patch equation $\sigma_1 = \sigma_i + kd^{(-1/2)}$, where d is grain size, σ_1 is yields stress, σ_i is material constant, and the tensile stress is inversely proportional to the grain size [47]. When the speed of rotating tool increases, the TIG welded metal unswervingly contacted with the tool experienced the most extensive plastic deformation. The number of new grains nucleation increases and forms large number of small grains due to increase in lattice distortion and intragranular dislocation density such that tensile strength of TIG + FSP welded

joint increases. When the tool rotational speed exceeded 1300 rpm, the turbulent flow arises at this moment and they could not produce high quality defect-free weld. The elongation of TIG + FSP welded joint is lower than both the base alloys. The decrease in elongation is due to the clustering of the strengthening precipitates, and also effect arising from the localization of strain occurs in the weld region during the friction stir processing [48].

Due to TIG + FSP approach with filler wire ER4043, the porosity, large grain size and presence of extra material are absent in the welded region, which shows the higher tensile strength than the conventional TIG joining process. The tensile strength of TIG welded joint was observed as 176.1 MPa, whereas maximum tensile strength (255 MPa) was found in TIG + FSP welded joint at 1300 rpm, 45 mm/min with tilt angle 1° as shown in Fig. 12 and Table 5.

3D responses surfaces plot and contour of tensile strength are shown in Fig. 13. When the tool rotation speed increases, tensile stress also increases due to strain hardening effect convinced by tool stirring, whereas excess heat input plays the predominant role at high tool rotation speed such as lower tensile strength was observed when the tool rotation decreases. As the feed rate increases, tensile strength first increases and then decreases. The minimum tensile strength, i.e., 185 MPa, was found at lower tool rotation speed (1000 rpm) due to inadequate tool stirring action [9]. The maximum tensile strength (255 MPa) was observed at 1300 rpm, 45 mm/min and 1° , when the feed rate or traverses speed increases, the tensile strength and hardness also increase up to a certain value. Large heat was found in the welded region at lower feed rate. As the feed rate increases, the influences of thermal cycle on the welded joint weakened leading to enhancement in tensile strength of the welded joints as shown in Fig. 13.

Fig. 12 Stress strain diagram of TIG+FSP welding, (a) tool rotation at 1000 rpm, (b) tool rotation at 1150 rpm and (c) tool rotation at 1300 rpm

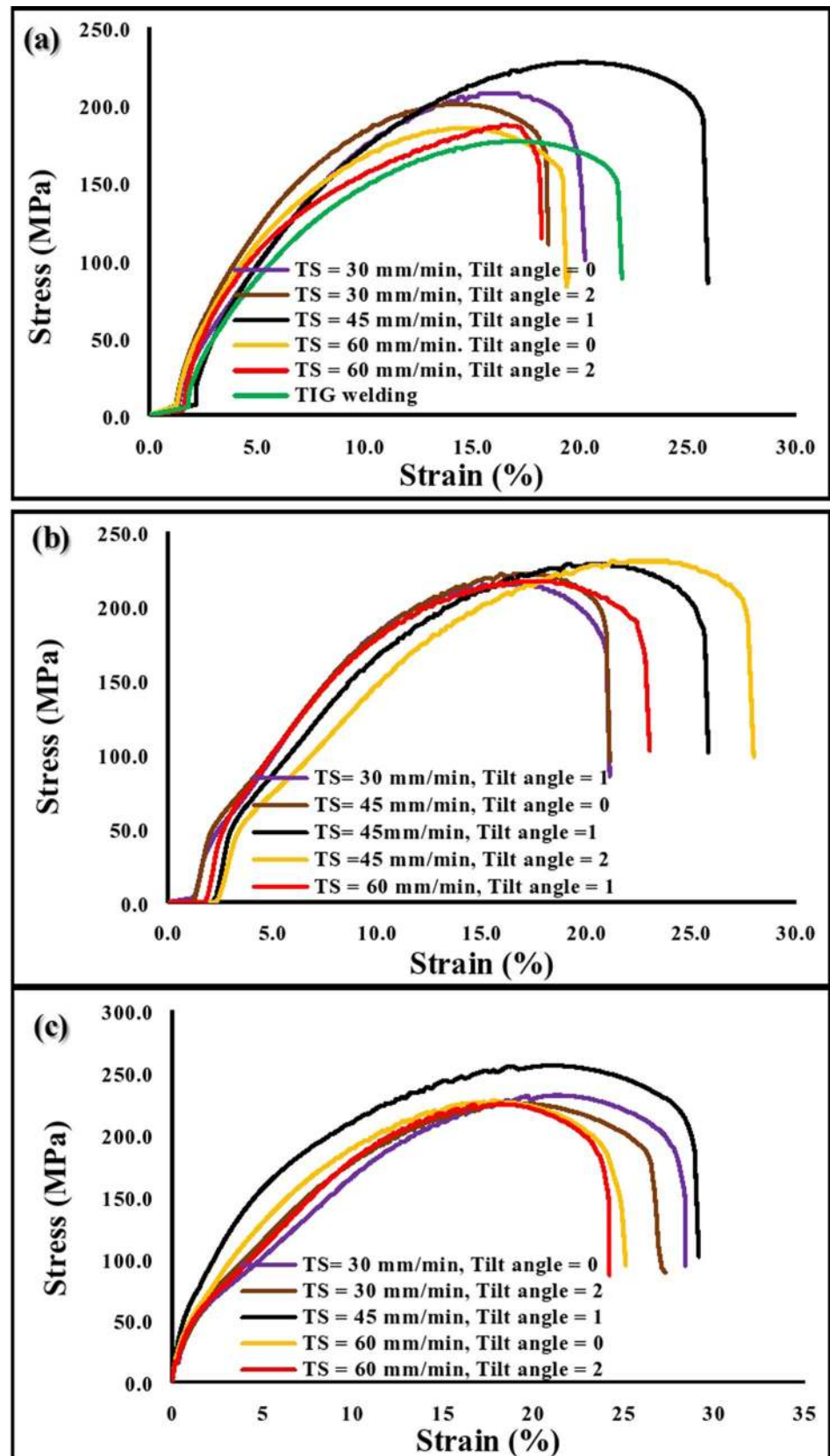


Table 5 Design experiment and their results

Sample	A: Tools rotations speeds (rpm)	B: Traverses speeds (mm/min)	C: Tilts angles (°)	UTS MPa	% E	Micro-hardness at nugget (HV)	Grain size (μm)
1	1150	45	2	230	28	100	6.4
2	1300	30	2	225	26.9	97	5.1
3	1150	45	1	225	28.1	95	6.2
4	1000	60	0	185	19.5	77	12.2
5	1000	45	1	228	25.9	94	6.7
6	1150	45	1	232	28.4	99	6.9
7	1000	30	0	207	20.2	81	10.5
8	1000	60	2	187	18.2	78	11.9
9	1150	45	1	233	27.5	101	5.7
10	1150	60	1	219	22.9	89	8.4
11	1300	60	0	226	25.1	93	5.8
12	1150	45	1	228	27.2	98	7.2
13	1150	45	1	232	26.1	99	4.9
14	1150	45	0	221	23.5	91	9.4
15	1300	60	2	224	24.2	91	10.3
16	1000	30	2	201	18.7	74	11.4
17	1150	30	1	214	21.1	87	10.8
18	1300	45	1	255	29.2	105	4.2
19	1300	30	0	231	28.4	101	6.3
20	1150	45	1	228	25.8	99	7.8

Micro-hardness

The micro-hardness distribution of TIG and TIG + FSP welded joint of AA6061 and AA7075 with different processing parameters was analyzed by Vickers hardness testing machine with a load of 100 g and dwell time 30 s are shown in Fig. 14. The micro-hardness values are asymmetrical in the weld center due to unsteady plastic flow and large grain structure in the weld center [49–51]. The alloying elements such as Si and Mg existing in weld center make precipitation reaction and form a strong precipitate of Mg_2Si to give a higher strength as shown in Fig. 11. It showed significant difference, where TIG welded joint using filler ER4043 showed a lower average hardness value compared to TIG + FSP joint. The maximum micro-hardness value, i.e., 105 HV, was obtained at the nugget zone of weldment with processing parameter TRS-1300, TS-45 and TA-1°. During welding, the filler wire ER4043 shows the columnar grains, while fine equiaxed grains are found in TIG + FSP welded joint. It may be analyzed that the fine equiaxed grains improve mechanical properties than the columnar grains [52].

Residual Stress Measurement by $\cos\alpha$ Method

For residual stress determination, the $\cos\alpha$ method was described [53–54]. The translation from the diffractometer space to the sample is inherently more complex due to the 2D planar geometry of the measurement and can be expressed as

$$q_s = \begin{bmatrix} \cos \eta \sin \psi_0 + \sin \eta \cos \psi_0 \cos \alpha \\ \cos \eta \sin \psi_0 \sin \phi_0 + \sin \eta \cos \psi_0 \sin \phi_0 \cos \alpha + \sin \eta \cos \phi_0 \sin \alpha \\ \cos \eta \cos \psi_0 + \sin \eta \sin \psi_0 \cos \alpha \end{bmatrix} \quad (1)$$

The strain projection along (η, α) coordinates can be written as in terms of scattering vector and strain component as

$$\begin{aligned} \varepsilon_\alpha &= q_i q_j \varepsilon_{ij} \\ \varepsilon_{ij} &= \frac{1+\nu}{E} \sigma_{ij} - \delta_{ij} \frac{\nu}{E} \sigma_{kk} \end{aligned} \quad (2)$$

So, the strain projection may be written as

$$\varepsilon_\alpha = \frac{1+\nu}{E} q_i q_j \sigma_{ij} - \frac{\nu}{E} \sigma_{kk} \quad (3)$$

Now, defining two parameter a_1 and a_2 for linear determination of σ_{11} and σ_{22}

$$a_1 = \frac{1}{2} [(\varepsilon_\alpha - \varepsilon_{\pi+\alpha}) + (\varepsilon_{-\alpha} - \varepsilon_{\pi-\alpha})] \quad (4)$$

$$a_2 = \frac{1}{2} [(\varepsilon_\alpha - \varepsilon_{\pi+\alpha}) - (\varepsilon_{-\alpha} - \varepsilon_{\pi-\alpha})] \quad (5)$$

After re-expressing of Eqs. (4) and (5) to lead the final relationship for this method.

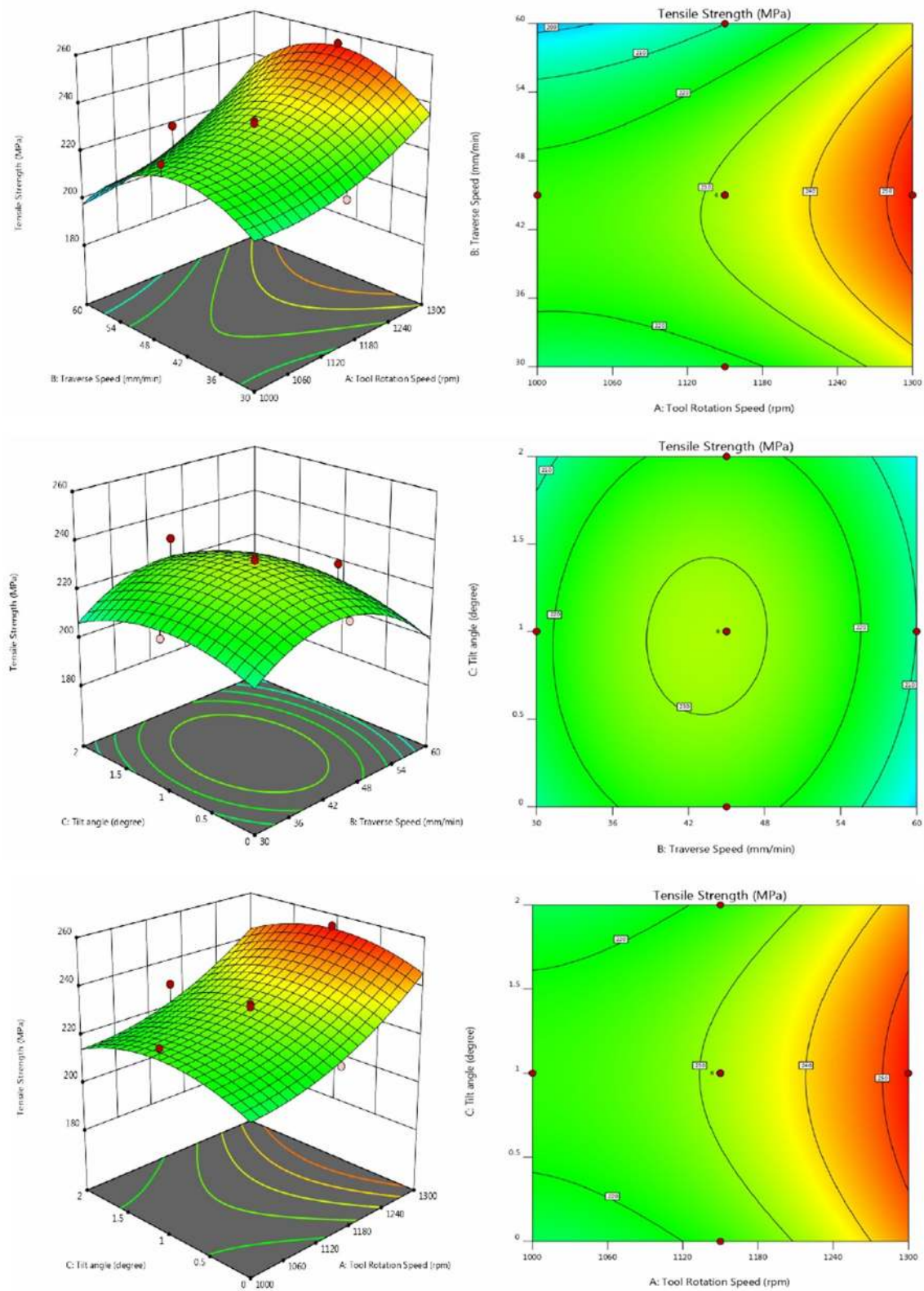
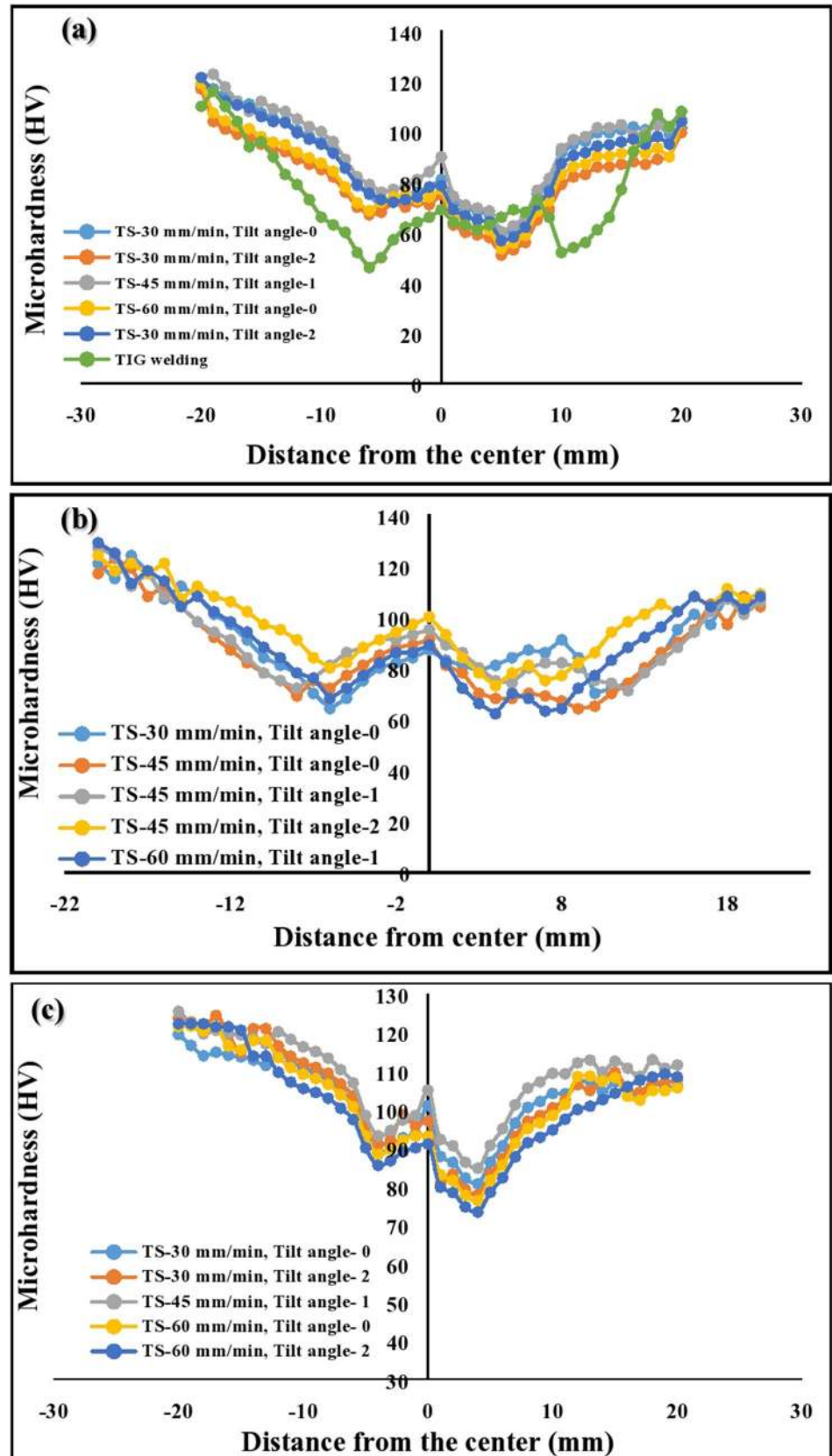


Fig. 13: 3D response surface plot and contour plot for tensile strength of TIG + FSP welded joint

Fig. 14 Distribution of microhardness of welded joint, (a) TIG welding, (b–d) TIG+FSP welded joint, (b) tool rotation 1000 rpm, (c) tool rotation 1150 rpm and (d) tool rotation 1300 rpm



$$a_1 = \frac{1+\nu}{E} \sin 2\psi_0 \sin 2\eta \cos \alpha [\sigma_{11}(1 + \cos 2\phi_0) + \sigma_{22}(1 - \cos 2\phi_0) + 2\sigma_{12}(\sin 2\phi_0)] \quad (6)$$

$$a_2 = \frac{1+\nu}{E} \sin \psi_0 \sin 2\eta \sin \alpha [\sigma_{22} \sin 2\phi_0 - \sigma_{11} \sin 2\phi_0 + 2\sigma_{12}(\cos 2\phi_0)] \quad (7)$$

at $\phi_0=0$, the above equations will be

$$a_1 = \sigma_{11} \frac{1+\nu}{E} \sin 2\psi_0 \sin 2\eta \cos \alpha \quad (8)$$

$$a_2 = 2\sigma_{11} \frac{1+\nu}{E} \sin \psi_0 \sin 2\eta \sin \alpha \quad (9)$$

Thus, the term $\cos \alpha$ in Eq. (8) is the origin of the name for this method.

The value of stresses after re-expression may be written as

$$\sigma_{11} = -\frac{E}{1+\nu} \frac{1}{\sin 2\psi_0 \sin 2\eta} \quad (10)$$

$$\sigma_{12} = -\frac{E}{2(1+\nu)} \frac{1}{\sin 2\psi_0 \sin^2 \eta} \quad (11)$$

Residual stresses (compressive or tensile) will influence the mechanical behavior of the welded joint. It can reduce brittle fracture strength, buckling strength and cracking in the weldment. Residual stress also influenced the prediction of brittle failure and affected the lifetime prediction of the component [55–57]. Residual stress contributes both negative and positive effects to the weldment. Generally, the tensile residual stress leads to negative effect to the weldment [45, 50]. A mini portable x-ray diffraction apparatus (Pulstec μ -X360) at Delhi technological university, Delhi, India, was used to determine the residual stresses in weldment of AA6061 and AA7075 by the $\cos \alpha$ method. The x-ray incident angle was set at 35° , and ± 5 oscillation was applied. The variation of residual stresses in transverse direction of TIG and TIG + FSP welded joint is shown in Fig. 15.

The base material AA7075 on LHS of the weldment shows a minimum compressive residual stress; however, the residual stress gradually increases from base material to toward the weldment and then decreases till second base material AA6061. The maximum compressive residual stress 77 MPa was located at the fusion zone (FZ) of the TIG weldment with filler ER4043, whereas minimum compressive residual stress 29 MPa was obtained at stir zone (SZ)

of the TIG + FSP. The residual stresses profile of TIG + FSP was not symmetrical about the centerline of the weldment for both the cases. The left side peak value of the weldment was greater than the right side, because the forming processes are different for retreating side (RS) and advancing side (AS).

Influence of Process Parameters on Residual Stress

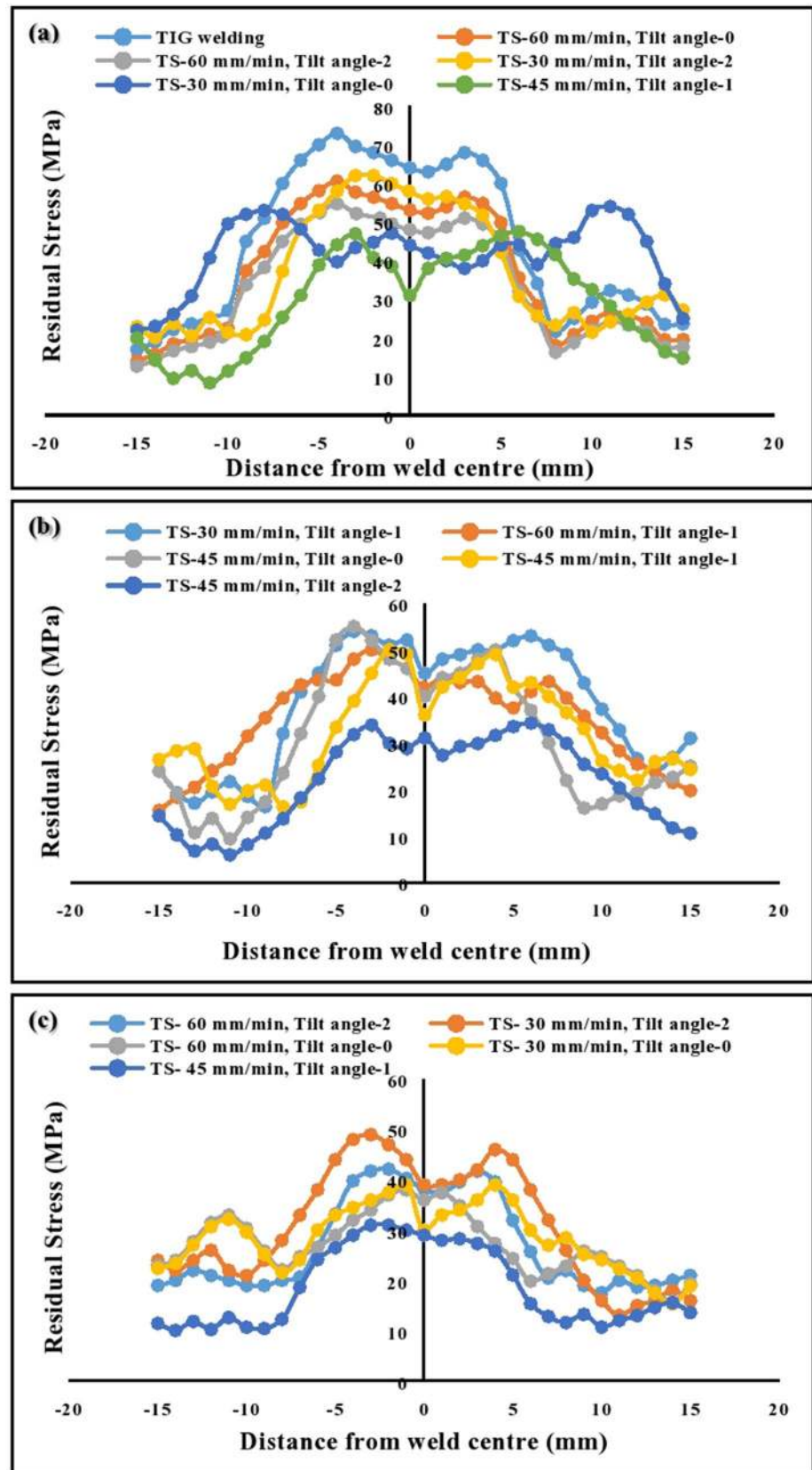
The value of residual stress is obtained by the experimental methods. Figure 15 shows a comparison between tool rotation and the compressive residual stress, grouped by traverse speed and tilt angle. It can be seen that the compressive residual stresses decrease for a given value of pitch as the traverse speed and tilt angle increase. According to [14], although measured peak residual stress increases with as traverse speed decreases, tensile stress appears to be limited to the softened weld zone instead, resulting in a narrowing of the tensile region [14]. The minimum value of compressive residual stress (29 MPa) is obtained at tool rotational speed of 1300 rpm, traverse speed 45 mm/min and tilt angle 1° . A 54.6% variation is observed in TIG welding and TIG + FSP welding. The trend in variation of maximum residual stress to the processing parameters is seen in Fig. 15.

Conclusions

The tensile strength, % elongation, micro-hardness at nugget zone and residual stress at nugget zone have been analyzed. The following conclusions are as follows:

- The FSP over the TIG welding completely modified the microstructure and mechanical properties of the TIG welded joint.
- The maximum tensile strength, percentage elongation and micro-hardness at nugget zone are 255 MPa, 29.2 and 105 HV at tool rotation 1300 rpm, traverse speed 45 mm/min and tilt angle 1° , whereas maximum residual stress (12.2 MPa) was found at tool rotation 1000 rpm, traverse speed 60 mm/min and tilt angle 0° .
- The application of FSP on TIG welded joint also improves the ductility of the welded joints; TIG + FSP welded joints are more ductile than the TIG welded joint due to fine grain structure.
- The grains size in the nugget zone in TIG + FSP welded joint was observed much finer ($4.2 \mu\text{m}$) than the TIG welded joint ($19.8 \mu\text{m}$).

Fig. 15 Variation of residual stress to the processing parameters of TIG+FSP, (a) tool rotation 1000 rpm, (b) tool rotation 1150 rpm and (c) tool rotation 1300 rpm



Conflict of interest The authors declare that they have no conflict of interest.

References

1. V.A. Mosneaga, T. Mizutani, T. Kobayashi, H. Toda, Impact toughness of weldments in Al-Mg-Si alloys. *Mater. Trans.* **43**, 1381–1389 (2002)
2. N. Karunakaran, Effect of pulsed current on temperature distribution and characteristics of GTA welded magnesium alloy. *IOSR J. Mech. Civ. Eng.* **4**, 1–8 (2013)
3. R.S. Mishra, Z.Y. Ma, Friction stir welding and processing. *Mater. Sci. Eng. Res.* **50**, 1–78 (2005)
4. M. Zhan, K. Guo, H. Yang, Advances and trends in plastic forming technologies for welded tubes. *Chin. J. Aeronaut.* **29**, 305–315 (2015)
5. K. Masubuchi, *Analysis of welded structures*, 1st edn. (Pergamon Press, New York, 1980)
6. C. Huang, S. Kou, Partially melted zone in aluminum welds liquation mechanism and directional solidification. *Weld. J.* **79**, 113–120 (2000)
7. A.P. Biddle, W.A. Wilson, Variable polarity plasma arc welding on the Space Shuttle external tank. *Weld. J.* **63**, 27–35 (1984)
8. G. Albertini, G. Bruno, B.D. Dunn, F. Fiori, W. Reimers, J.S. Wright, Comparative neutron and x-ray residual stress measurements on Al-2219 welded plate (1997). *Mater. Sci. Eng. A* **224**, 157–165 (1997)
9. W. Xu, J. Liu, G. Luan, C. Dong, Microstructure and mechanical properties of friction stir welded joints in 2219-T6 aluminum alloy. *Mater. Des.* **30**, 3460–3467 (2009)
10. R. P. Matrukanitz, in *Selection and weldability of heat-treatable aluminium alloys*. ASM Hand Book Welding, Brazing, and Soldering, vol. 6. (ASM International, Cleveland, 1993) pp. 528–536
11. C.G. Rhodes, M.W. Mahoney, W.H. Bingel, Effects of friction stir welding on microstructure of 7075 aluminium. *Scr. Mater.* **36**, 69–75 (1997)
12. J.Q. Su, T.W. Nelson, R. Mishra, M. Mahoney, Microstructural investigation of friction stir welded 7050-T651 aluminium. *Acta Mater.* **51**, 713–729 (2003)
13. M. Zhan, K. Guo, H. Yang, Advances and trends in plastic forming technologies for welded tubes. *Chin. J. Aeronaut.* **29**, 305–315 (2015)
14. M. Peel, A. Steuwer, M. Preuss, P.J. Withers, Microstructure, mechanical properties and residual stresses as a function of welding speed in aluminium AA5083 friction stir welds. *Acta Mater.* **51**, 4791–4801 (2003)
15. T. Li, Q. Y. Shi, H. K. Li, W. Wang, and Z. P. Cai, in *Residual stresses of friction stir welded 2024 T-4 joints*. International Welding Joining Conference-Korea (2007).
16. M.A. Sutton, A.P. Reynolds, D.Q. Wang, C.R. Hubbard, A Study of residual stresses and microstructure in 2024-T3 aluminum friction stir butt welds. *J. Eng. Mater. Technol.* **124**, 215–221 (2002)
17. W.B. Lee, Mechanical properties related to micro structural variation of 6061 Al alloy joints by friction stir welding. *J. Mater. Trans.* **45**, 1700 (2004)
18. K. Elangovan, V. Balasubramanian, Influences of pin profile and rotational speed of the tool on the formation of friction stir processing zone in AA2219 aluminium alloy. *J. Mater. Sci. Eng. A* **459**, 7–18 (2007)
19. K. Elangovan, V. Balasubramanian, Influences of tool pin profile and axial force on the formation of friction stir processing zone in AA6061 aluminium alloy. *Int. J. Adv. Manuf. Technol.* **38**, 285–295 (2008)
20. H. Mehdi, R.S. Mishra, Mechanical properties and microstructure studies in Friction Stir Welding (FSW) joints of dissimilar alloy—a review. *J. Achiev. Mater. Manuf. Eng.* **77**, 31–40 (2016)
21. H. Mehdi, R.S. Mishra, Influences of process parameter and microstructural studies in friction stir welding of different alloys: a review. *Int. J. Adv. Prod. Ind. Eng.* **5**, 55–62 (2017)
22. H. Mehdi, R.S. Mishra, Mechanical and microstructure characterization of friction stir welding for dissimilar alloy—a review. *Int. J. Res. Eng. Innov.* **1**, 57–67 (2017)
23. Y.K. Periyasamy, A.V. Perumal, B.K. Periyasamy, Optimization of process parameters on friction stir welding of AA7075-T651 and AA6061 joint using response surface methodology. *Mater. Res. Express* **6**, 96558–96584 (2019)
24. M. Jayaraman, R. Sivasubramanian, V. Balasubramanian, A.K. Lakshminarayanan, Prediction of tensile strength of friction stir welded A356 cast aluminium alloy using response surface methodology and artificial neural network. *J. Manuf. Sci. Prod. Res.* **9**, 1–21 (2008)
25. S. Rajakumar, C. Muralidharan, V. Balasubramanian, Optimization of the friction stir- welding process and the tool parameters to attain a maximum tensile strength of AA7075-T6 aluminium alloy. *J. Eng. Manuf.* **224**, 1175–1191 (2010)
26. A.K. Lakshminarayanan, V. Balasubramanian, Process parameters optimization for friction stir welding of RDE-40 aluminum alloy using Taguchi technique, Transactions of Nonferrous Metals Society of China. *Trans. Nonferrous Met. Soc. China* **18**, 548–554 (2008)
27. H. G. Neddermeijer, G. J. van Oortmarssen, N. Piersma, R. Dekker, in *A framework for response surface methodology for simulation optimization*. Proceeding Winning Simulation Conference, vol. 128 2000. 129 136
28. C. Pandey, M.M. Mahapatra, P. Kumar, F. Daniel, N. Saini, Dissimilar joining of CSEF steels using autogenous tungsten-inert gas welding and gas tungsten arc welding and their effect on δ -ferrite evolution and mechanical properties. *J. Manuf. Proc.* **31**, 247–259 (2018)
29. C. Pandey, M.M. Mahapatra, P. Kumar, N. Saini, Comparative study of autogenous tungsten inert gas welding and tungsten arc welding with filler wire for dissimilar P91 and P92 steel weld joint. *Mater. Sci. Eng. A* **712**, 720–737 (2017)
30. Pk Chaurasia, C. Pandey, A. Giri, N. Saini, M.M. Mahapatra, A comparative study of transverse shrinkage stresses and residual stresses in P91 welded pipe including plasticity error. *Arch. Metall. Mater.* **63**, 1000–1011 (2018)
31. L. Zhou, R.X. Zhang, X.Y. Hu, N. Guo, H.H. Zhao, Y.X. Huang, Effects of rotation speed of assisted shoulder on microstructure and mechanical properties of 6061-T6 aluminum alloy by dual-rotation friction stir welding. *Int. J. Adv. Manuf. Technol.* **100**, 199–208 (2018)
32. K. Devireddy, V. Devuri, M. Cheepu, B.K. Kumar, Analysis of the influence of friction stir processing on gas tungsten arc welding of 2024 aluminum alloy weld zone. *Int. J. Mech. Prod. Eng. Res. Dev.* **8**, 243–252 (2018)
33. S. Mabuwa, V. Msomi, Review on friction stir processed TIG and friction stir welded dissimilar alloy joints. *Adv. Mater. Sci. Eng.* **2019**, 142–159 (2019)
34. S. Kou, *Welding Metallurgy*, 2nd edn. (Wiley, New York, 2003)
35. W. Tang, X. Guo, J.V. Mclure, L.E. Murr, Heat input and temperature distribution in friction stir welding. *J. Mater. Process. Manuf. Sci.* **7**, 163–172 (1998)
36. D. Yi, T. Onuma, S. Mironov, Y.S. Sato, H. Kokawa, Evaluation of heat input during friction stir welding of aluminium alloys. *Sci. Technol. Weld. Join.* **22**, 41–46 (2016)

37. M.W. Mahoney, C.G. Rhodes, J.G. Flintoff, W.H. Bingel, R.A. Spurling, Properties of friction-stir-welded 7075 T651 aluminum. *Metall. Mater. Trans. A* **29**, 1955–1964 (1998)
38. H.J. Mohammadzadeh, H. Farahani, M.K.G. Besharati, M.V. Aghaei, Study on the effects of friction stir welding process parameters on the microstructure and mechanical properties of 5086-H34 aluminum welded joints. *Int. J. Adv. Manuf. Technol.* **83**, 611–621 (2016)
39. Ş. Kasman, Z. Yenier, Analyzing dissimilar friction stir welding of AA5754/AA7075. *Int. J. Adv. Manuf. Technol.* **70**, 145–156 (2014)
40. G. Liu, R. Xin, J. Li, D. Liu, Q. Liu, Fracture localization in retreating side of friction stir welded magnesium alloy. *Sci. Tech. Weld. Join.* **205**, 378–384 (2015)
41. S.H. Good, I.M. Brown, The nucleation of cavities by plastic deformation. *Acta Mater.* **27**, 1–15 (1979)
42. T.C. Tszeng, Interfacial stresses and void nucleation in discontinuously reinforced composites. *J. Eng. Mater. Technol.* **122**, 86–92 (2000)
43. C. Pandey, M.M. Mahapatra, P. Kumar, P. Kumar, N. Saini, J.G. Thakare, S. Kumar, Study on effect of double austenitization treatment on fracture morphology tensile tested nuclear grade P92 steel. *Eng. Fail. Anal.* **96**, 158–167 (2018)
44. C. Pandey, N. Saini, M.M. Mahapatrab, P. Kumar, Study of the fracture surface morphology of impact and tensile tested cast and forged (C&F) Grade 91 steel at room temperature for different heat treatment regimes. *Eng. Fail. Anal.* **71**, 131–147 (2017)
45. V. Patel, V. Badheka, A. Kumar, Influence of friction stir processed parameters on superplasticity of Al-Zn-Mg-Cu alloy. *Mater. Manuf. Process.* **31**, 1573–1582 (2016)
46. K.T. Senthil, V. Balasubramanian, M.Y. Sanavullah, Influences of pulsed current tungsten inert gas welding parameters on the tensile properties of AA 6061 aluminium alloy. *Mater. Des.* **28**, 2080–2092 (2007)
47. Y. Li, A.J. Bushby, D.J. Dunstan, The Hall–Petch effect as a manifestation of the general size effect. *Proc. R. Soc. A* **472**, 20150890 (2016)
48. S.N. Shanmuga, N. Murugan, Tensile behavior of dissimilar friction stir welded joints of aluminium alloys. *Mater. Des.* **31**, 4184–4193 (2010)
49. W. Xu, J. Liu, G. Luan, C. Dong, Temperature evolution, microstructure and mechanical properties of friction stir welded thick 2219-O aluminum alloy joints. *Mater. Des.* **30**, 1886–1893 (2009)
50. W. Xu, J. Liu, G. Luan, C. Dong, Microstructure and mechanical properties of friction stir welded joints in 2219–T6 aluminum alloy. *Mater. Des.* **30**, 3460–3467 (2009)
51. T. Luijendijk, Welding of dissimilar aluminium alloys. *J. Mater. Proc. Technol.* **103**, 29–35 (2000)
52. M. Ishak, N.F.M. Noordin, L.H.A. Shah, Feasibility study on joining dissimilar aluminum alloys AA6061 and AA7075 by tungsten inert gas (TIG). *Jurnal Teknolo* **75**, 79–84 (2015)
53. R. Nandan, G.G. Roy, T.J. Lienert, T. Debroy, Three-dimensional heat and material flow during friction stir welding of mild steel. *Acta Mater.* **55**, 883–895 (2007)
54. S. Taira, K. Tanaka, T. Yamazaki, A method of x-ray microbeam measurement of local stress and its application to fatigue crack growth problem. *J. Soc. Mater. Sci. Jpn.* **27**, 251–256 (1978)
55. K. Jitender, S. Hari, 2018 Modelling and analysis of process parameters in friction stir welding of AA5083-H321 using response surface methodology. *Adv. Mater. Proc. Technol.* **4**, 183–199 (2018)
56. W. J. Arbogast, Modeling friction stir joining as a metal working process, in *Symposium, Hot Deformation of Aluminum Alloys*, San Diego, CA, 2003, pp. 313–330
57. M.N.M. Salleh, M. Ishak, L.H. Shah, S.R.A. Idris, The effect of ER4043 and ER5356 filler metal on welded Al 7075 by metal inert gas welding. *WIT Trans. Built. Environ.* **166**, 213–224 (2016)

Publisher's Note Springer Nature remains neutral with regard to jurisdictional claims in published maps and institutional affiliations.